Tool speed and polarity effects in micro-EDM drilling of 316L stainless steel

Cyril Pilligrin, J.; Asokan, P.; Jerald, J.; Kanagaraj, G.; Mukund Nilakantan, J.; Nielsen, Izabela

Published in:
Production and Manufacturing Research

DOI (link to publication from Publisher):
10.1080/21693277.2017.1357055

Publication date:
2017

Document Version
Publisher's PDF, also known as Version of record

Taylor & Francis
Taylor & Francis Group

Production & Manufacturing Research
An Open Access Journal

ISSN: (Print) 2169-3277 (Online) Journal homepage: http://www.tandfonline.com/loi/tpmr20

Tool speed and polarity effects in micro-EDM drilling of 316L stainless steel

J. Cyril Pilligrin, P. Asokan, J. Jerald, G. Kanagaraj, J. Mukund Nilakantan & Izabela Nielsen

To cite this article: J. Cyril Pilligrin, P. Asokan, J. Jerald, G. Kanagaraj, J. Mukund Nilakantan & Izabela Nielsen (2017) Tool speed and polarity effects in micro-EDM drilling of 316L stainless steel, Production & Manufacturing Research, 5:1, 99-117, DOI: 10.1080/21693277.2017.1357055

To link to this article: https://doi.org/10.1080/21693277.2017.1357055

Published online: 25 Jul 2017.

PRODUCTION & MANUFACTURING RESEARCH, 2017
VOL. 5, NO. 1, 99–117
https://doi.org/10.1080/21693277.2017.1357055

Taylor & Francis
Taylor & Francis Group

Tool speed and polarity effects in micro-EDM drilling of 316L stainless steel

J. Cyril Pilligrin[a], P. Asokan[a], J. Jerald[a], G. Kanagaraj[b], J. Mukund Nilakantan[c] and Izabela Nielsen[c]

[a]Department of Production Engineering, National Institute of Technology, Tiruchirappalli, India; [b]Department of Mechanical Engineering, Thiagarajar College of Engineering, Madurai, India; [c]Department of Materials and Production, Aalborg University, Aalborg, Denmark

ABSTRACT

This paper focuses on the issues of Resistor-Capacitor-based Electrical Discharge Micro-Machining process and investigates the effects of tool speed and polarity on the performance measures such as Tool Wear Rate, Material Removal Rate, Overcut and Taper Angle by drilling on 316L Stainless Steel. Taguchi's L54 mixed orthogonal array design is employed to conduct experiments by varying tool polarity at two levels and voltage, capacitance, spindle speed at three levels. The cause and effect relationship between the experimental factors and responses are analysed and discussed using Factorial Analysis of Variance technique. Optimum combinations of machining parameters are also evaluated using Taguchi-based Grey Relational Analysis, by considering grey relational grade matrix and influence of process parameters on the responses. Further, microscopic analysis is done to identify the micro-voids, globular formation, and cracks present on the surface of the hole produced under various machining conditions.

ARTICLE HISTORY
Received 23 May 2017
Accepted 10 July 2017

KEYWORDS
Micro-machining; EDM; polarity; Taguchi; grey relational analysis

1. Introduction

In today's industrial scenario, removal of materials in a micro-metre range is an essential requirement to make precise components (Jain, 2014). Micro-holes which are created for various automobile components, optical devices, and medical instruments must be so accurate in dimensions, in order to use in sensitive applications (Chung, Shin, Park, Kim, & Chu, 2011; Masuzawa, 2000). Micro-components are used in marine fields for detecting volatile gases and organic compounds to screen biological molecules (Tonacci, Corda, Tartarisco, Pioggia, & Domenici, 2014). Such micro-components are fabricated by various micro-fabrication techniques (Kibria, Bhattacharyya, & Davim, 2017). Among them, Electrical Discharge Micro-Machining (EDMM) is a well-known micro-fabrication technique that has an ability to produce complicated profiles (Prakash, Kansal, Pabla, Puri, & Aggarwal, 2016). Irrespective of the hardness of the materials, any conductive material

CONTACT G. Kanagaraj gkmech@tce.edu

can be machined by EDMM process (Unune, Singh, & Mali, 2016). EDMM is also known as spark erosion process in which work material is eroded by electrical sparks so that mechanical stresses and vibrations problems are very less.

In this research work, the experiments are conducted to analyse the machining characteristics of EDMM process by changing the tool and work polarity and also varying the tool rotational speed. The effects of process parameters on the machining characteristics such as TWR, MRR, taper angle and overcut is also investigated while drilling micro-holes on SS 316L material. This material has wide applications like valve spools, damper plates, aerospace nozzle guide segments, combustion liners, medical and textile needles. Experiments are conducted based on Taguchi's L54 mixed orthogonal array design by varying the tool polarity at two levels and voltage, capacitance, spindle speed at three levels. In addition, the cause-and-effect relationship between the experimental factors and responses are analysed using Factorial ANOVA technique. Also, the optimum combinations of machining parameters are evaluated using Taguchi-based Grey Relational Analysis (GRA), by considering the grey relational grade matrix and the influence of process parameters on the responses. Further, microscopic analysis is done to identify the micro-voids, globular formation and cracks present on the surface of the hole produced under various machining conditions.

The rest of this paper is structured as follows. Section 2 reviews the related works in the area of EDM process. Later on, Section 3 describes the experimental set-up details to perform micro-holes on 316L Stainless Steel. The effects of tool speed and polarity on the performance measures and geometrical characteristics are discussed in Section 4. The details of ANOVA, GRA and SEM analysis is presented in Section 5. Finally, the concluding remarks are drawn in the last section together with the future research directions.

2. Literature review

EDMM process performance is measured in terms of TWR, MRR, overcut, taper angle and surface integrity. In order to improve these performance measures, the EDMM process needs to be studied in detail. Only a few researchers have addressed the phenomenon of drilling micro-holes by EDMM. Raju, Srinivasa, Vinod, and Chellamalai (2013) analysed the influence of electrode diameter and capacitance on the MRR, surface roughness (SR), volumetric wear ratio and spark gap. Kibria, Sarkar, Pradhan, and Bhattacharyya (2010) examined the effect of dielectrics and stated that MRR and TWR were found to be lower for Kerosene than the Deionized water. Liu et al. (2016) studied the impact of input parameters and electrode shape on various performance measures of die-sinking EDM and found that electrode geometry had a critical role in the performance. Tseng, Kao, and Chang (2016) developed a real-time monitoring system for EDMM process which is capable of producing nano-silver particles in the form of debris and compared the particle size with the conventional EDM process. Li, Hou, Xu, and Yu (2016) investigated the micro-holes drilled by three different EDM drilling methods and found that better MRR and TWR is achieved for cutting edge electrodes.

Wong, Rahman, Lim, Han, and Ravi (2003) analysed the material removal mechanism of EDMM process using single pulse discharges and stated that high efficiency was obtained at lower energy levels. Lee, Kim, and Kim (2015) improved the efficiency of the EDMM process by vibrating the workpiece at low frequency and identified that the short circuits that occur during machining are reduced and proper flushing occurs due to low-frequency vibration.

Guo et al. (2014) analysed the material removal mechanism of the EDMM by integrating two temperature and molecular dynamics model. They found that initially the material is removed in bulk, from the cathode due to thermal shock and later the material is removed in single atoms. Manivannan and Kumar (2017) improved the machining performance of the EDMM process by cooling the machining environment with the cryogenic coolant and found that it has significantly improved the MRR and TWR. Selvarajan, Manohar, Kumar, and Dhinakaran (2017) studied the effects of EDM process parameters on various responses by drilling holes on Si_3N_4-TiN ceramic composites. They have modelled the EDM process using multiple regression analysis and also found the optimum combination using grey relational analysis.

Literature review shows that there are many research efforts reported in the area of EDM-die sinking process based on the transistor-type pulse generator. But there are limited literature on EDM-drilling based on resistance–capacitance-type pulse generator where the effects of tool speed and polarities are not studied. Depending upon the circuit type used in the machine, the effect of parameters is also varied and the stochastic thermal nature of the EDM process makes it difficult to explain all of those effects fully. The debris removal from the inter-electrode gap is one of the reasons for more MRR in μEDM. If there is no proper debris removal, higher spark energy produces results in higher amount of debris. This debris sticking on the workpiece trapped in and causes unwanted spark. The un-wanted sparks erodes materials from the tool electrode, which results high tool wear. Thus, a great portion of discharge energy occupies with unwanted sparking, while the remaining erodes the work material (Ali, Mehfuz, Khan, & Ismail, 2012). Hence, in this research work investigations are done to analyse the various issues of EDMM process by changing the tool polarity and also varying the tool rotational speed. The experiments were carried out by drilling several micro-holes using different process parameters, namely tool polarity, tool speed, peak current and voltage. Some process performance indicators, such as TWR, MRR, and geometric indicators such as diametric overcut and taper angle were taken into account.

3. Experimental set-up details

In this work, DT110–Multiprocess Micro-machining centre (Figure 1) (Make: Mikrotools Pvt. Ltd., Singapore) was used to drill micro-holes on SS 316L workpiece by EDMM process. It is a 3-axes CNC servo controlled machine which is energized by RC pulse generator. The maximum travel range of this machine is 200 mm in X-axis, 100 mm in Y-axis and 100 mm in Z-axis with a resolution of .1 μm in all directions and also has a full closed-feedback control that ensures sub-micron accuracy. The EDMM set-up consists of a cylindrical electrode rigidly fixed in the spindle and the workpiece material is clamped on a fixture. The spindle can rotate up to 5000 rpm with the help of variable speed spindle drive. During machining, both the workpiece and the tool are immersed in the dielectric fluid. An external flushing system is used to circulate the dielectric and to provide proper flushing. The work material, electrode material and dielectric used in this study were 316L stainless steel of size 25 × 25 × .5 mm, ϕ .3 mm tungsten rod and DCO-1000i EDM oil, respectively, and their corresponding properties are listed in Tables 1–3. The experimental conditions are listed in Table 4.

The performance of the EDMM process depends on various factors like voltage, capacitance, speed, feed rate, dielectric, flushing pressure, polarity, etc. Among these tool polarity,

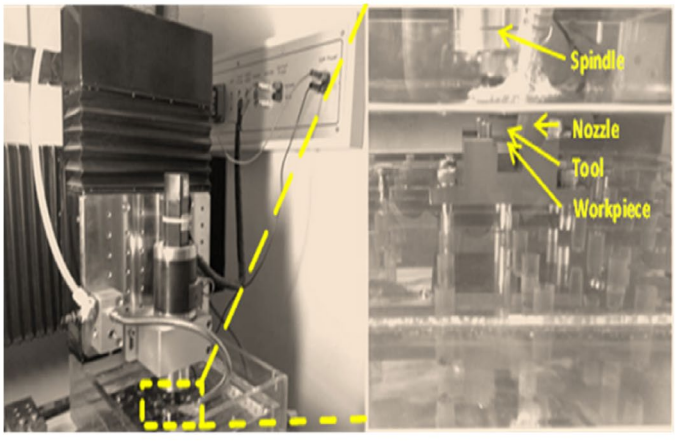

(a)

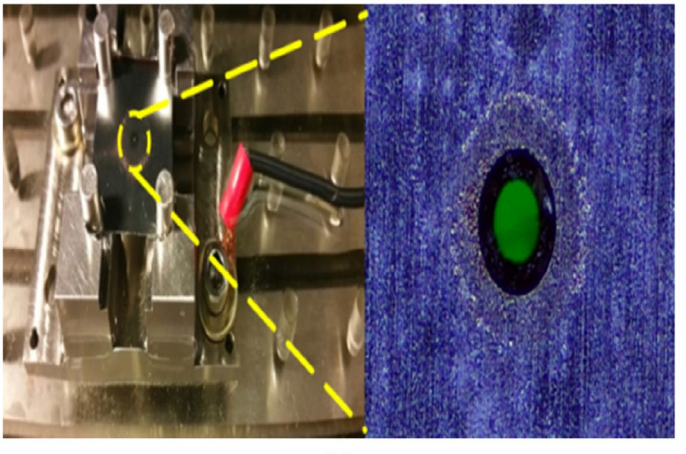

(b)

Figure 1. (a) EDMM experimental set-up. (b) SS316L Work material on the fixture.

Table 1. Material properties of SS 316L.

Properties	Values
Density (kg/m^3)	8000
Tensile strength (MPa)	485
Thermal conductivity (W/m-K)	21.5
Brinell hardness (HRB)	95
Specific heat (J/kg-K)	500

Table 2. Properties of electrode materials.

	Density	Brinell hardness	Thermal conductivity	Melting point
Composition	(kg/m^3)	(HRB)	(W/m-K)	(K)
Pure W (99.9%)	19.25	115	173	3695

Table 3. Properties of dielectric fluid.

Properties	Values
Specific gravity	.81
Flash point (°C)	100
Viscosity (mm^2/s)	2.53
Appearance	Colourless transparent liquid

Table 4. Micro-electrical discharge drilling experimental conditions.

Parameters	Particulars
Resistance	1 KΩ
Feed rate	1.0 µm/s
Polarity of the tool	Positive (P), negative (N)
Voltage (V)	100, 120, 140
Capacitance (nF)	.01, .10, .40
Tool speed (rpm)	0, 250, 500

spindle speed, voltage and capacitance are the primary factors which affect the performance of EDMM. Hence, these four factors are taken as inputs for the experimental design. To study the effects of each factor and to find its ranges, the experiments are conducted based on full factorial design (Montgomery, 2013) with two replications. Totally 54 (L54) experiments have been conducted with three factors (speed, voltage and capacitance) at three levels and one factor (tool polarity) at two levels for each replication as shown in Table 5.

The workpiece and tool mass is measured using an analytical balance having a repeatability of .00002 g (Make: Contech CA184), before and after machining. The entry and exit hole diameters are assessed by Non-contact video measurement system (ARCS KIM1510E). The TWR, MRR, Overcut and Taper angle is selected as output responses to measure the performance characteristics. The equations used to calculate those output responses are given below (Karthikeyan, Ramkumar, Dhamodaran, & Aravindan, 2010; Mathew, Somashekhar, Sooraj, Subbarao, & Ramachandran, 2009). In this study, three replicated tests were conducted. The mean value of three tests was taken as the final value which is used for calculating the response values (MMR, TWR, overcut and taper angle) and for ANOVA analysis. The mean values of these output responses are shown in Table 5.

$$\text{MRR}\left(\text{mm}^3/\text{min}\right) = \frac{\text{Amount of material removal from workpiece}}{\text{drilling time}} \tag{1}$$

$$\text{TWR}\left(\text{mm}^3/\text{min}\right) = \frac{\text{Volume of material removal from electrode}}{\text{drilling time}} \tag{2}$$

$$\text{Overcut (mm)} = \frac{\text{Entry Hole Diameter} - \text{Tool Diameter}}{2} \tag{3}$$

$$\text{Taper angle}\left(\text{deg.}\right) = \tan^{-1}\left(\frac{\text{Entry Hole Diameter} - \text{Exit Hole Diameter}}{2 \times \text{Height of the workpiece}}\right) \tag{4}$$

Table 5. Experimental results.

Exp. No.	Tool polarity	Voltage (V)	Capacitance (nF)	Tool speed (rpm)	MRR (mm^3/min)	TWR (mm^3/min)	Overcut (mm)	Taper angle (deg.)
1	N	100	.01	0	4.7124	18.6463	.026	19.44
2	N	100	.01	250	5.9458	11.3695	.021	12.00
3	N	100	.01	500	4.9364	22.1606	.023	16.92
4	N	100	.1	0	9.7862	24.0272	.039	28.46
5	N	100	.1	250	16.6552	16.7325	.036	20.97
6	N	100	.1	500	13.7236	31.6359	.039	24.56
7	N	100	.4	0	33.7090	36.9663	.062	38.47
8	N	100	.4	250	47.6520	21.5312	.056	32.03
9	N	100	.4	500	41.4339	51.0088	.059	35.51
10	N	120	.01	0	4.6178	25.5280	.030	23.99
11	N	120	.01	250	8.4450	15.1775	.025	15.87
12	N	120	.01	500	6.7987	30.7471	.027	18.42
13	N	120	.1	0	13.2327	31.0206	.049	29.10
14	N	120	.1	250	24.8049	21.0104	.044	21.92
15	N	120	.1	500	19.5609	38.2536	.047	25.01
16	N	120	.4	0	45.1475	43.4007	.068	40.68
17	N	120	.4	250	60.3223	25.2935	.064	34.69
18	N	120	.4	500	52.4111	57.5405	.066	37.79
19	N	140	.01	0	6.6548	31.3345	.038	28.30
20	N	140	.01	250	14.6320	25.4921	.032	20.69
21	N	140	.01	500	9.6819	39.0967	.035	23.30
22	N	140	.1	0	21.8993	42.2876	.055	36.99
23	N	140	.1	250	32.9619	28.4146	.052	27.40
24	N	140	.1	500	29.2236	49.1097	.053	32.66
25	N	140	.4	0	51.7252	67.2417	.072	45.31
26	N	140	.4	250	65.6906	41.4257	.070	38.15
27	N	140	.4	500	58.7516	72.7619	.072	40.40
28	P	100	.01	0	2.9857	9.5015	.020	6.99
29	P	100	.01	250	4.1250	4.4806	.017	4.86
30	P	100	.01	500	3.9741	5.7020	.018	5.71
31	P	100	.1	0	10.4823	12.8404	.034	16.57
32	P	100	.1	250	17.1859	6.4191	.031	11.22
33	P	100	.1	500	14.5863	10.3236	.033	14.31
34	P	100	.4	0	25.9800	19.0305	.059	24.70
35	P	100	.4	250	37.9833	11.6990	.054	18.27
36	P	100	.4	500	30.6318	15.3354	.057	21.75
37	P	120	.01	0	3.4744	12.8064	.025	10.86
38	P	120	.01	250	6.6722	7.9528	.024	8.65
39	P	120	.01	500	5.1314	8.9377	.025	9.48
40	P	120	.1	0	11.8506	15.1067	.044	19.80
41	P	120	.1	250	21.1627	9.7963	.037	13.48
42	P	120	.1	500	16.9732	13.9881	.043	17.29
43	P	120	.4	0	35.6407	22.7576	.063	26.79
44	P	120	.4	250	49.4417	14.4859	.059	20.41
45	P	120	.4	500	41.0169	18.0431	.061	23.34
46	P	140	.01	0	5.3881	14.3641	.030	13.22
47	P	140	.01	250	10.4602	9.4059	.026	11.68
48	P	140	.01	500	7.4281	10.1355	.029	13.68
49	P	140	.1	0	16.6524	17.4196	.051	23.03
50	P	140	.1	250	27.6763	10.9995	.047	16.29
51	P	140	.1	500	21.1868	15.7118	.048	21.54
52	P	140	.4	0	42.4951	24.3190	.067	29.47
53	P	140	.4	250	55.1436	16.4804	.065	23.81
54	P	140	.4	500	49.8620	21.1333	.066	26.03

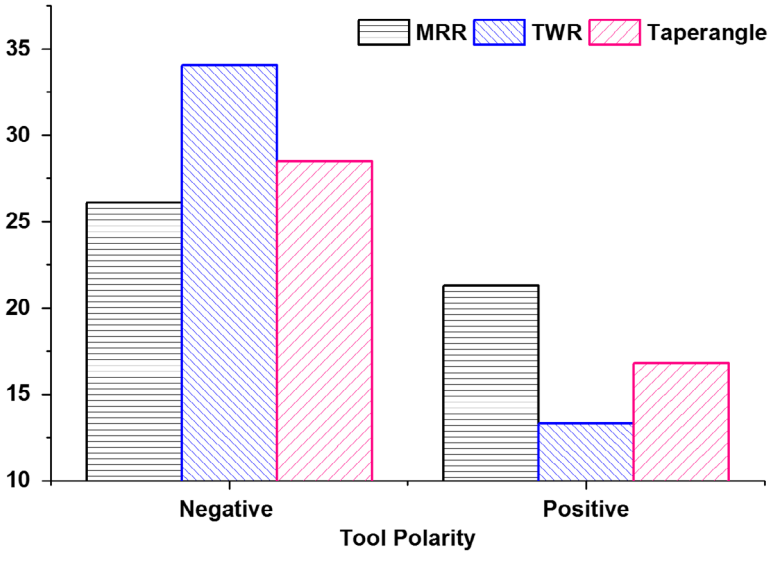

Figure 2. Effects of polarity on process parameters.

4. Results and discussion

In this section, the influence of various EDMM process parameters on output responses like MRR, TWR, Taper angle and Overcut are discussed. The discussion is based on the experimental results obtained by drilling micro-holes on SS 316L material and Factorial ANOVA analysis performed on it.

4.1. Effects of polarity

Figure 2 indicates the results related to MRR, TWR and Taper angle response changes due to polarity effects. It can be noticed that the MRR is increases for tool negative than the tool positive, because of more amount of electrons are discharged from the tool. These electrons strike the workpiece at high velocity and produce more amount of heat at the IEG. Hence, work material is eroded from the top substrate due to melting and evaporation (Jerald, Kumanan, Kumar, & Chandrakar, 2013). It can also be inferred from the Figure 3 that the melting volume of tool negative is larger than the tool positive. This volume difference is due to the variation in amount of heat generated (Nakajima, Okada, & Uno, 1991).

It can also be seen from the Figure 4 that the tool shape differs abnormally in negative polarity this is due to crack propagation resulting from rapid heat cycle and deposition of metal on the tool surface. Hence, the tool wear for negative polarity is much higher than the positive polarity. When the TWR is more, the shape of the tool also gets altered; hence, the machined micro-hole becomes tapered. For tool positive, the TWR and the taper angle is small and for tool negative the TWR is more, so taper angle is also higher.

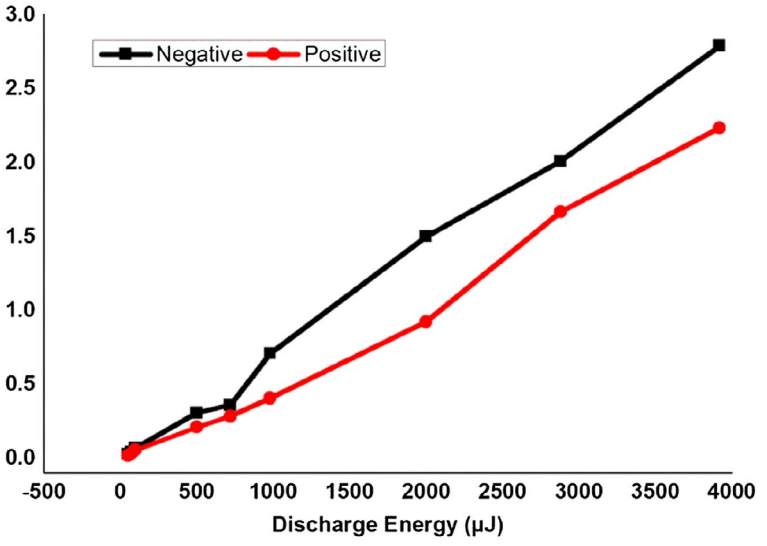

Figure 3. Relation between discharge energy and melting volume.

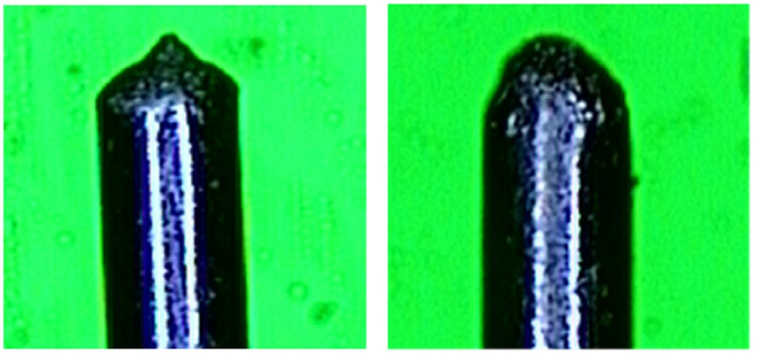

Figure 4. Tungsten tool after machining at 120 V, .10nF and 100 rpm. (a) Tool negative. (b) Tool positive.

4.2. Effects of tool speed

Generally in EDMM process, the tool remains stationary, but in this work tool speed is also considered with various speeds. The tool speed produces centrifugal effect on the dielectric and it causes the movement of debris particles that are present in the IEG. When the spindle speed is increased, proper flushing of debris occurs due to centrifugal effect and hence there is a reduction in machining time (Cyril, Paravasu, Jerald, Sumit, & Kanagaraj, 2017). From the Figure 5, it is observed that MRR is high during better flushing conditions. Beyond a certain limit of tool speed, the movement of debris becomes faster and it causes instability by producing secondary sparks in the IEG, thus MRR is decreased but TWR, Taper angle and overcut are increased (Figure 6).

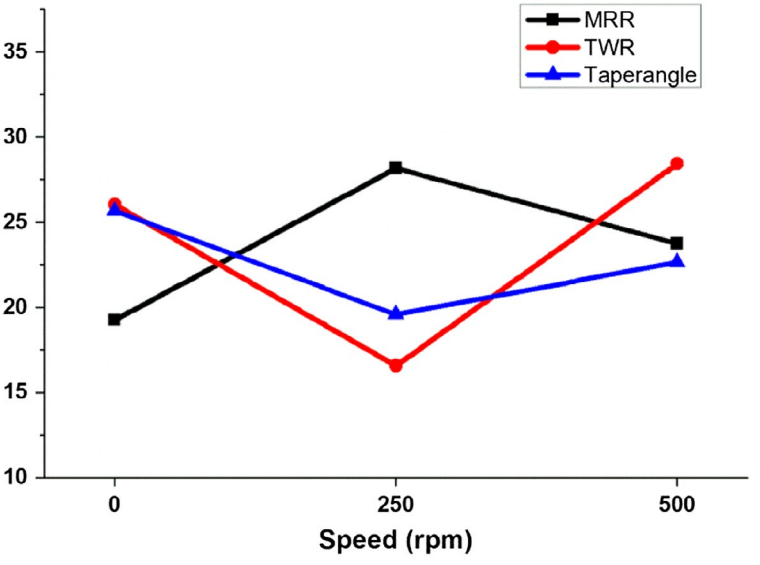

Figure 5. Effects of tool speed on process parameters.

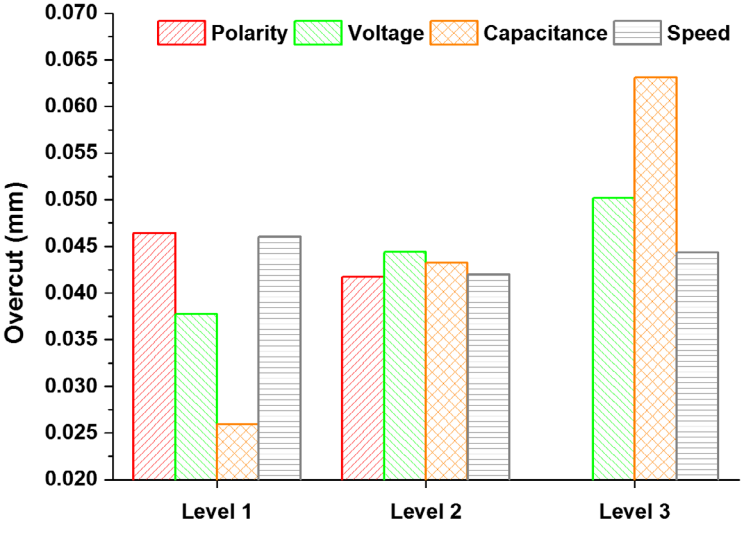

Figure 6. Effects of process parameters on overcut.

At zero rpm, the tool remains stationary and there is no centrifugal effect. Hence, the debris doesn't have any movements which cause instability and improper flushing. Due to this, more secondary sparks and short circuits occur; hence, machining time is also increased.

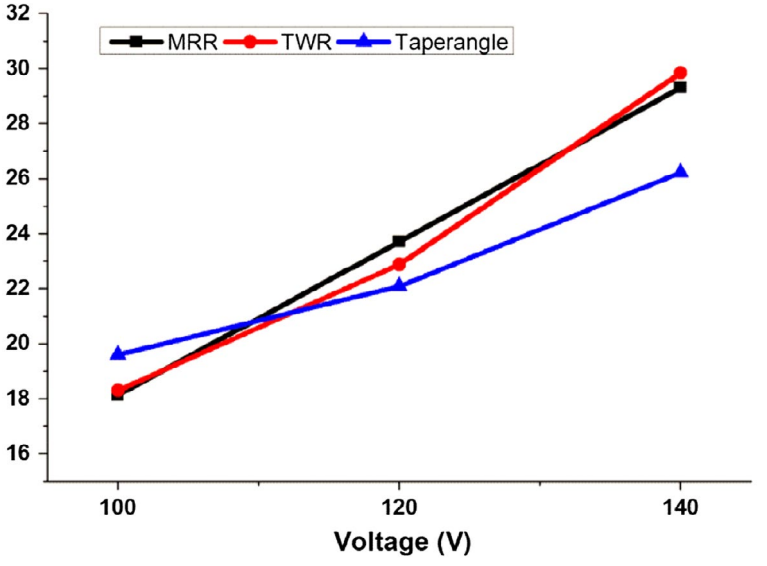

Figure 7. Effects of voltage on process parameters.

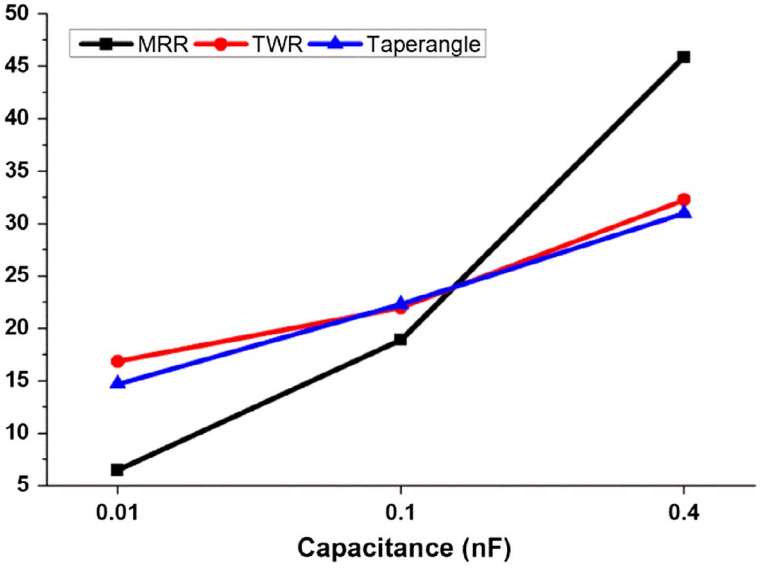

Figure 8. Effects of capacitance on process parameters.

4.3. Effects of voltage and capacitance

The voltage and capacitance directly contribute to discharge energy of the RC-based EDMM process. The following equation is used to calculate discharge energy (Jain, 2014).

$$\text{Discharge energy}\,(\mu\text{J}) = \frac{\text{capacitance} \times \text{voltage}^2}{2} \tag{5}$$

when there is an increase in capacitance and voltage from lower levels, the discharge energy also gets increased. Hence, more heat is generated at the IEG. At high levels of voltage and capacitance the MRR and TWR are higher (Figures 7 and 8) due to high discharge energy.

5. Analysis of the results

5.1. Factorial ANOVA analysis

The factorial ANOVA computes the degree to which combination of independent variables used to predict the values of dependent variables (English, 2006). It also analyse the cause-and-effect relationship between the experimental factors. The ANOVA analysis on MRR, TWR, Overcut and Taper angle is done and the results are listed in Table 6. It shows the influence of input parameters on output responses. The ratio between explained and total variation is defined as coefficient of determination (R^2) and it is also a measure of degree of fitness (Torres, Puertas, & Luis, 2016). For MRR, the R^2 value is 96.05%, which indicates the model variability. Whereas R^2_{adj} value is 95.45%, which indicates the correlation between the MRR and process parameters are well characterized by the developed model. When *P*-value of a parameter is less than .05 at 95% confidence level, the corresponding parameter is significant and has individual effect on the output responses (Khan, Khan, Siddiquee, Chanda, & Arindam, 2014). It is seen from the Table 6 that the *P*-value of all the parameters are less than .05 at 95% confidence interval for output responses. Thus, all individual parameters are significant on MRR, TWR, Overcut and Taper angle.

5.2. Regression analysis

In general, a true functional relationship between dependent variables (responses) and independent variables (input factors) are unknown. This relationship between variables can be established by a mathematical model called regression model. It is an empirical model which expresses the results of the experiments quantitatively, to facilitate understanding, implementation and interpretation (Montgomery, 2013). Hence, this section focuses on establishing a truly functional relationship by fitting linear regression models. In general, the dependent variable *y* may be related to k independent variables as given below.

$$Y = \beta_0 + \beta_1 X_1 + \beta_2 X_2 + \beta_3 X_3 + \ldots\ldots + \beta_p X_p + \varepsilon \quad (6)$$

Table 6. Results of ANOVA for process parameters.

		For MRR		For TWR		For overcut		For taper angle	
Factors	DoF	Adj. SS	*P*-value	Adj. SS	*P*-value	Adj. SS	*P*-value	Adj. SS	*P*-value
Polarity	1	310.68	.00	5808.21	.00	.00030	.00	1846.88	.00
Voltage	2	1122.53	.00	1215.59	.00	.00140	.00	402.80	.00
Capacitance	2	14,597.43	.00	2221.10	.00	.01247	.00	2397.10	.00
Speed	2	715.81	.00	1415.99	.00	.00015	.00	334.81	.00
Error	46	687.88		2009.48		.00017		71.11	
Total	53	17,434.33		12,670.37		.00442		1664.58	
R^2		96.05%		84.14%		99.31%		97.70%	
$R^2_{adj.}$		95.45%		81.73%		99.21%		97.34%	

Notes: DoF – degrees of freedom; Adj. SS – adjusted sum of squares.

This is a multiple linear regression model with 'p' independent variables. These independent variables are also called as predictor variables. Where β_i, $i = 0, 1, 2\ldots p$, are called regression coefficients. This model describes a hyper plane in the p-dimensional space of the independent variables (Li et al., 2016). The parameter β_i represents the expected change in response y per unit change in X_i when all the remaining independent variables X_j ($j \neq i$) are held constant. The derived multi-linear regression model for all output responses are as follows:

$$\begin{aligned}\text{MRR} = &-21.53 - \left(4.80 \times \text{ToolPolarity}\right) + \left(.2792 \times \text{Voltage}\right) + \left(98.20 \times \text{Capacitance}\right) \\ &+ \left(.00899 \times \text{Speed}\right)\end{aligned} \tag{7}$$

$$\begin{aligned}\text{TWR} = &\ 12.47 - \left(20.74 \times \text{Tool Polarity}\right) + \left(.2885 \times \text{Voltage}\right) + \left(38.23 \times \text{Capacitance}\right) \\ &+ \left(.00478 \times \text{Speed}\right)\end{aligned} \tag{8}$$

$$\begin{aligned}\text{Overcut} = &-.00032 - \left(.00470 \times \text{Tool Polarity}\right) \\ &+ \left(.000311 \times \text{Voltage}\right) + \left(.08803 \times \text{Capacitance}\right) - \left(.000003 \times \text{Speed}\right)\end{aligned} \tag{9}$$

$$\begin{aligned}\text{Taper angle} = &\ 15.26 - \left(11.696 \times \text{ToolPolarity}\right) + \left(.1656 \times \text{Voltage}\right) \\ &+ \left(38.60 \times \text{Capacitance}\right) - \left(.00605 \times \text{Speed}\right)\end{aligned} \tag{10}$$

5.3. Grey relational analysis

Taguchi's design with ANOVA can only predict the effects and relationship of the process parameters over the output responses. Since the data obtained from the above design are discrete in nature, uncertainties are more which will have a complex interaction effect on the performance characteristics. These uncertainties are solved using GRA which has certain advantages over the other statistical techniques (Kundu & Singh, 2016). In GRA, multi-objective problems are transformed into a single objective problem. Thus, Taguchi design with GRA remains most potent method to solve multi-objective optimization problems (Yadav, Yadava, & Singh, 2014). The GRA processing steps are listed below (Pannerselvam, 2012).

Step 1: Initially, the raw data are pre-processed. The normalized values of the responses are calculated based on the following equations. The MRR which is higher the better performance variable thus the normalization equation (Sarkar, Panja, Das, & Sarkar, 2015) is expressed as:

$$Y_{pq} = \left(\frac{X_{pq} - \text{Min}\left(X_{pq}\right)}{\text{Max}\left(X_{pq}\right) - \text{Min}\left(X_{pq}\right)} \right) \tag{11}$$

The TWR, Overcut and Taper angle which are lower the better performance variable thus the normalization equation is expressed as:

$$Y_{ij} = \left(\frac{\text{Max}\left(X_{pq}\right) - X_{pq}}{\text{Max}\left(X_{pq}\right) - \text{Min}\left(X_{pq}\right)} \right) \tag{12}$$

where X_{pq} = measured responses, min (X_{pq}) = minimum of X_{pq} and max (X_{pq}) = maximum of X_{pq}, p = response variables and q = trial number (number of the experiments). Fundamentally larger the normalized values, better the performance characteristics.

Step 2: The maximum of the Y_{pq} regardless of responses and trials are computed by the following equation.

$$\text{Reference value } (R) = \text{ Max } \left(Y_{pq} \right) \tag{13}$$

Step 3: The absolute variance between the reference value R and each normalized value is computed as follows:

$$\Delta_{pq} = \left| Y_{pq} - R \right| \tag{14}$$

where R is the expected sequence, Y_{pq} is the comparability sequence and Δ_{pq} is the deviation sequence of R and Y_{pq}.

Step 4: The Grey Relation Coefficient (GRC) ξ_{pq} for each of the normalized values is computed using the following equation.

$$\xi_{pq} = \left(\frac{\text{Min } \left(\Delta_{pq} \right) + \zeta \text{ Max } (\Delta_{pq})}{\Delta_{pq} + \zeta \text{ Max } (\Delta_{pq})} \right) \tag{15}$$

where ζ is the differentiating coefficient $\zeta \in [0, 1]$ and Deng (2002) has stated that .5 is the most widely accepted value. The amount of relational degree between the actual and desired performance characteristics can be obtained through GRC values, ranging from 0 to 1. Higher the GRC value, the more intense is the relational degree.

Step 5: The Grey Relation Grade (GRG) for each trial is computed as follows:

$$\gamma_j = \frac{\sum_{i=1}^{n} \xi_{pq}}{n} \tag{16}$$

where n denotes number of response variables. The computed GRC and GRG values are summarized in Table 7. The level of relationship between comparability and reference sequence is shown by the GRG. Combinations of machining parameters with higher GRG values are the desired optimum multi performance characteristics (Chakravorty, Gauri, & Chakraborty, 2013). The GRG value for trail no. 29 has the largest values among the others GRG values. The optimum combination of the process parameters obtained from the mean GRG table is polarity: positive, voltage: 100 v, capacitance: 0.01 nF, tool speed: 250 rpm as highlighted in Table 8.

After obtaining the optimum combination of process parameters from GRA, the final step is to run a validation experiment for the results attained by the Taguchi's design. A confirmation experiment is necessary only when the obtained optimum combination is not one of the trail runs. In this case, the obtained optimum combination is one of the trail runs of the full factorial experiments, so a confirmation experiment is not conducted. A significant improvement in experimental GRG implies that this method can be utilized for multi-objective optimization of EDMM process. The ANOVA

Table 7. Grey relation grade.

	GRC values					
Sl. No.	MRR	TWR	OC	Taper angle	GRG	GRG rank
1.	.34	.71	.76	.58	.5956	20
2.	.34	.83	.86	.74	.6939	6
3.	.34	.66	.81	.63	.6090	15
4.	.36	.64	.55	.46	.5022	40
5.	.39	.74	.59	.56	.5690	23
6.	.38	.56	.56	.51	.4994	41
7.	.50	.51	.38	.38	.4405	51
8.	.63	.67	.42	.43	.5360	35
9.	.56	.42	.40	.40	.4456	50
10.	.34	.62	.68	.51	.5382	33
11.	.35	.76	.78	.65	.6347	13
12.	.35	.57	.73	.60	.5592	25
13.	.37	.56	.46	.45	.4630	46
14.	.43	.67	.50	.54	.5381	34
15.	.40	.50	.48	.50	.4722	45
16.	.60	.47	.35	.36	.4456	49
17.	.85	.62	.37	.40	.5620	24
18.	.70	.39	.36	.38	.4584	48
19.	.35	.56	.57	.46	.4847	44
20.	.38	.62	.64	.56	.5505	27
21.	.36	.50	.60	.52	.4946	43
22.	.42	.47	.42	.39	.4242	54
23.	.49	.59	.44	.47	.4981	42
24.	.46	.43	.43	.42	.4372	52
25.	.69	.35	.33	.33	.4277	53
26.	1.00	.48	.34	.38	.5505	28
27.	.82	.33	.34	.36	.4625	47
28.	.33	.87	.90	.90	.7530	3
29.	.34	1.00	1.00	1.00	.8344	1
30.	.34	.97	.95	.96	.8027	2
31.	.36	.80	.61	.63	.6030	16
32.	.39	.95	.66	.76	.6910	7
33.	.38	.85	.63	.68	.6357	12
34.	.44	.70	.40	.50	.5112	37
35.	.53	.83	.43	.60	.5966	19
36.	.47	.76	.41	.54	.5456	30
37.	.34	.80	.77	.77	.6689	9
38.	.35	.91	.79	.84	.7210	4
39.	.34	.88	.78	.81	.7040	5
40.	.37	.76	.50	.58	.5520	26
41.	.41	.87	.58	.70	.6386	11
42.	.39	.78	.51	.62	.5761	22
43.	.51	.65	.37	.48	.5038	38
44.	.66	.77	.40	.57	.5981	18
45.	.56	.72	.38	.52	.5455	32
46.	.34	.78	.68	.71	.6265	14
47.	.36	.87	.74	.75	.6822	8
48.	.35	.86	.70	.70	.6505	10
49.	.39	.73	.45	.53	.5228	36
50.	.45	.84	.48	.64	.6027	17
51.	.41	.75	.47	.55	.5455	31
52.	.57	.63	.36	.45	.5038	39
53.	.75	.74	.37	.52	.5927	21
54.	.66	.67	.36	.49	.5461	29

results for GRG are listed in Table 9. The polarity, voltage, capacitance and speed have a significant effect on the multi-performance characteristics. The capacitance (34.85%) influences more on the multi-performance characteristics followed by polarity (31.56%), speed (14.30%) and voltage (9.23%).

Table 8. Response table of the GRG.

Level	Polarity	Voltage	Capacitance	Speed
1	.5145	**.6036**	**.6446**	.5315
2	**.6205**	.5655	.5428	**.6161**
3		.5335	.5151	.5550
Delta	.1060	.0701	.1295	.0846
Rank	2	4	1	3

Table 9. Results of ANOVA for GRG.

Factors	DoF	Adj. SS	MSS	*P*-value	% contribution
Polarity	1	.1516	.1516	.00	31.56
Voltage	2	.0443	.0222	.00	9.23
Capacitance	2	.1674	.0837	.00	34.85
Speed	2	.0687	.0343	.00	14.30
Error	46	.0483	.0011		10.06
Total	53	.4804			100.00
R^2			89.94%		
$R^2_{adj.}$			88.41%		

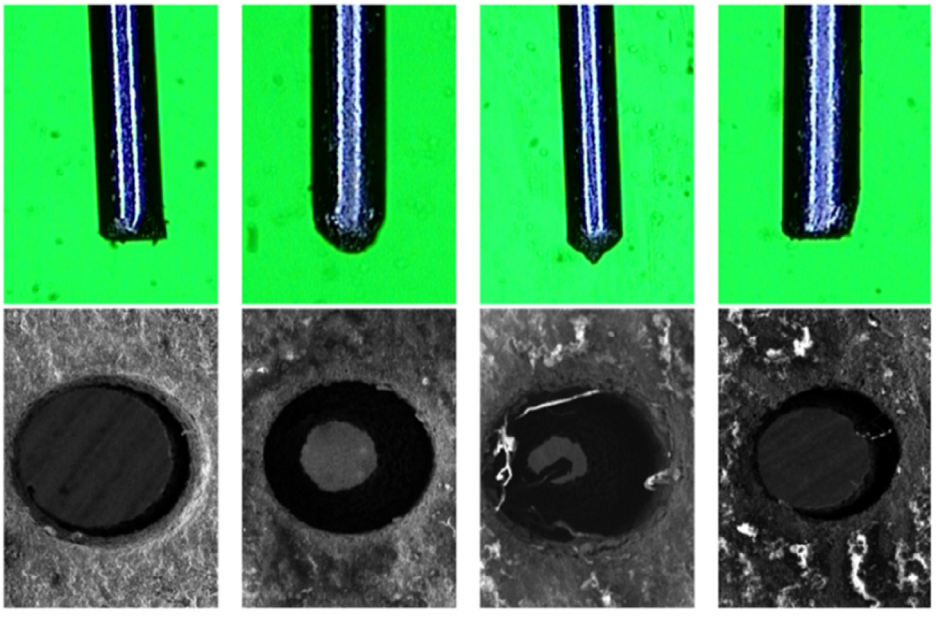

Figure 9. SEM images at magnification level of 100X for different machining conditions with the corresponding tool electrode. (a) In Tool positive, 120 V, .01nF and 100 rpm. (b) In Tool positive 140 V, .01nF and 500 rpm. (c) In Tool negative 140 V, .10nF and 500 rpm. (d) Tool negative, 100 V, .10nF and 100 rpm.

5.4. SEM analysis

The machined surfaces have been analysed using HITACHI S3000H Scanning Electron Microscope (SEM) to identify the influence of process parameters on surface characteristics. From the Figure 9(a) and 9(d), it is clear that at low discharge energy the holes produced

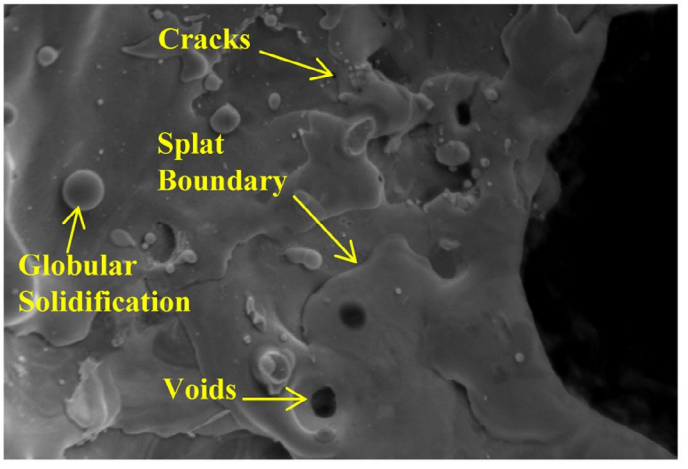

Figure 10. SEM images at magnification level of 1000× for Tool positive 140 V, .40 nF and 100 rpm.

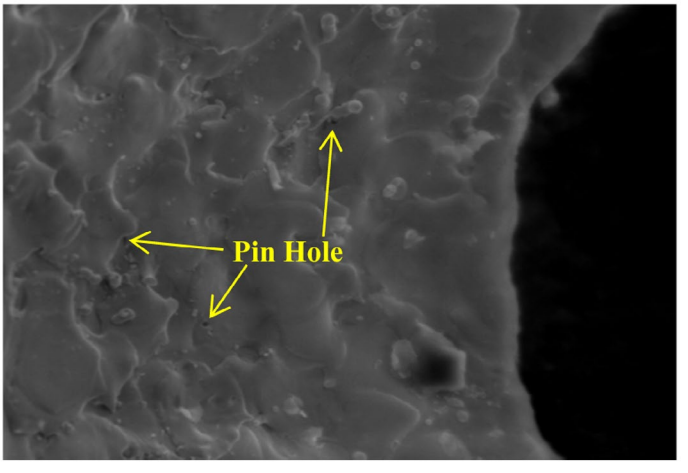

Figure 11. SEM images at magnification level of 1000× for Tool positive, 120 V, .01 nF and 100 rpm.

are smooth and the circularity of the hole is better. At high voltage and capacitance (Figure 9(b) and 9(c)), the discharge energy is more, so that heat generated is also more and the heat dissipation rate is inadequate. Thus, the gases formed at the machining area are unable to escape which leads to the formation of voids (Figure 10) on the machined surfaces. Due to the implosion of some gas bubbles, a few amount of material from the dielectric and tool electrode are deposited on the machined surfaces. Also the machined surfaces are cooled suddenly due to recharging of the dielectric during pulse off time, which produces a temperature difference between the substrates of the machined surfaces. Hence, cracks are formed due to this temperature gradient (Figure 11).

6. Conclusive remarks

In this study, the effect of straight and reverse tool polarities and tool speed on the machining performance of 316L Stainless steel using micro-electrical discharge drilling process was analysed. The voltage, capacitance, speed and feed rate were the varied machining parameters. The performance was evaluated in terms of MRR, TWR, Overcut and Taper angle. Based on results and discussion of the conducted experimental study, the following conclusions are derived:

- In tool negative polarity, the number of electrons hitting the workpiece is more than the electrons hitting the tool electrode. Thus, MRR is high and TWR is low.
- At zero rpm, the machining conditions are unstable due to improper flushing and evacuation of debris. Hence, MRR is low and TWR is high compared to other machining conditions. Due to proper evacuation of debris and flushing of dielectric, the overcut is smaller at the speed of 250 rpm.
- The cause and effect relationship of process parameters on performance characteristics are analysed using ANOVA technique. The ANOVA analysis of GRG shows that capacitance (34.85%) influences more on the multi-performance characteristics followed by polarity (31.56%), speed (14.30%) and voltage (9.23%). Hence, proper selection of process parameters is very important for EDMM.
- From the average GRG, it is found that the highest value of GRG is for the Positive Polarity, Voltage 100 V, Capacitance .01nf and Spindle Speed 250 rpm. It is the optimum combination of process parameters for the EDMM process with maximum MRR and minimum TWR, overcut and taper angle.

This research study can be extent further to analyse the various process parameters of different pulse generators on MRR, surface integrity, TWR, heat-affected zone (HAZ), taper angle, surface crack density (SCD), overcut and white layer thickness (WLT). Development of a comprehensive thermal model based on the superheating theory which uses realistic boundary conditions such as Gaussian distributed heat flux, temperature dependent thermal properties and expending plasma radius is another interesting area for research. Finite element model can be created to study the material removal, tool wear procedure and to analyse the cause and effects of HAZ, SCD and WLT.

Disclosure statement

No potential conflict of interest was reported by the authors.

ORCID

J. Cyril Pilligrin http://orcid.org/0000-0003-0117-6588

References

Ali, M. Y., Mehfuz, R., Khan, A. A., & Ismail, A. F. (2012). Micro eletro discharge milling for microfabrication. In *Micromachining techniques for fabrication of micro and nano structures* (pp. 131–158). InTech.

Chakravorty, R., Gauri, S. K., & Chakraborty, S. (2013). A study on the multi-response optimisation of EDM processes. *International Journal of Machining and Machinability of Materials, 13*, 91–109.

Chung, D. K., Shin, H. S., Park, M. S., Kim, B. H., & Chu, C. N. (2011). Recent researches in micro electrical machining. *International Journal of Precision Engineering and Manufacturing, 12*, 371–380.

Cyril, J., Paravasu, A., Jerald, J., Sumit, K., & Kanagaraj, G. (2017). Experimental investigation on performance of additive mixed dielectric during micro-electric discharge drilling on 316L stainless steel. *Materials and Manufacturing Processes, 32*, 638–644.

Deng, J. (2002). *The fundamentals of grey theory*. Wuhan: Huazhong University of Science and Technology Press.

English, F. W. (2006). *Encyclopedia of educational leadership and administration*. Thousand Oaks, CA: Sage.

Guo, J., Zhang, G., Huang, Y., Ming, W., Liu, M., & Huang, H. (2014). Investigation of the removing process of cathode material in micro-EDM using an atomistic-continuum model. *Applied Surface Science, 315*, 323–336.

Jain, V. K. (2014). *Introduction to micromachining*. New Delhi: Narosa Publishing House.

Jerald, J., Kumanan, S., Kumar, S. P. L., & Chandrakar, H. V. (2013). Experimental investigation and optimisation of process parameters in micro-electrical discharge machining. *International Journal of Manufacturing Technology and Management, 27*, 88–100.

Karthikeyan, G., Ramkumar, J., Dhamodaran, S., & Aravindan, S. (2010). Micro electric discharge milling process performance: An experimental investigation. *International Journal of Machine Tools and Manufacture, 50*, 718–727.

Khan, N. Z., Khan, Z. A., Siddiquee, A. N., Chanda, A. K., & Arindam, K. (2014). Investigations on the effect of wire EDM process parameters on surface integrity of HSLA: A multi-performance characteristics optimization. *Production & Manufacturing Research, 2*, 501–518.

Kibria, G., Bhattacharyya, B., & Davim, J. P. (Eds.). (2017). *Non-traditional micromachining processes*. Cham: Springer International Publishing.

Kibria, G., Sarkar, B. R., Pradhan, B. B., & Bhattacharyya, B. (2010). Comparative study of different dielectrics for micro-EDM performance during microhole machining of Ti-6Al-4 V alloy. *The International Journal of Advanced Manufacturing Technology, 48*, 557–570.

Kundu, J., & Singh, H. (2016). Friction stir welding: Multi-response optimisation using Taguchi-based GRA. *Production & Manufacturing Research, 4*, 228–241.

Lee, P. A., Kim, Y., & Kim, B. H. (2015). Effect of low frequency vibration on micro EDM drilling. *International Journal of Precision Engineering and Manufacturing, 16*, 2617–2622.

Li, Y., Hou, W., Xu, J., & Yu, H. (2016). *An investigation on drilling micro holes in different processes using micro-EDM*. Proceedings of 2016 IEEE International Conference on Mechatronics and Automation (pp. 1283–1288). Harbin, China.

Liu, Q., Zhang, Q., Zhu, G., Wang, K., Zhang, J., & Dong, C. (2016). Effect of electrode size on the performances of micro-EDM. *Materials and Manufacturing Processes, 31*, 391–396.

Manivannan, R., & Kumar, M. P. (2017). Improving the machining performance characteristics of the μEDM drilling process by the online cryogenic cooling approach. *Materials and Manufacturing Processes,* 1–7.

Masuzawa, T. (2000). State of the art of micromachining. *CIRP Annals – Manufacturing Technology, 49*, 473–488.

Mathew, J., Somashekhar, K. P., Sooraj, V. S., Subbarao, N., & Ramachandran, N. (2009). Effect of work material and machining conditions on the accuracy and quality of micro holes. *International Journal of Abrasive Technology, 2*, 279–298.

Montgomery, D. C. (2013). *Design and analysis of experiments*. New Delhi: PHI Learning Private Limited.

Nakajima, T., Okada, M., & Uno, Y. (1991). The effect of electrode polarity on electrical discharge machining performance in water. *Memoirs of the Faculty of Engineering, 26*, 9–20.

Pannerselvam, R. (2012). *Design and analysis of experiments*. New Delhi: PHI Learning Private Limited.

Prakash, C., Kansal, H. K., Pabla, B. S., Puri, S., & Aggarwal, A. (2016). Electric discharge machining – A potential choice for surface modification of metallic implants for orthopedic applications: A review. *Proceedings of the Institution of Mechanical Engineers, Part B: Journal of Engineering Manufacture, 230*, 331–353.

Raju, V. R., Srinivasa, C. K., Vinod, A. R., & Chellamalai, M. (2013). *Studies on micro-electrical discharge machining of steel using copper electrodes*. National Conference on Micro and Nano Fabrication (Vol. 1, pp. 1–5). Bangalore.

Sarkar, A., Panja, S. C., Das, D., & Sarkar, B. (2015). Developing an efficient decision support system for non-traditional machine selection: An application of MOORA and MOOSRA. *Production & Manufacturing Research, 3*, 324–342.

Selvarajan, L., Manohar, M., Kumar, A. U., & Dhinakaran, P. (2017). Modelling and experimental investigation of process parameters in EDM of Si3N4-TiN composites using GRA-RSM. *Journal of Mechanical Science and Technology, 31*, 111–122.

Tonacci, A., Corda, D., Tartarisco, G., Pioggia, G., & Domenici, C. (2014). A smart system to detect volatile organic compounds produced by hydrocarbons on seawater. In *Lecture Notes in Electrical Engineering* (Vol. 268, pp. 99–102).

Torres, A., Puertas, I., & Luis, C. J. (2016). EDM machinability and surface roughness analysis of INCONEL 600 using graphite electrodes. *The International Journal of Advanced Manufacturing Technology, 84*, 2671–2688.

Tseng, K. H., Kao, Y. -S., & Chang, C. -Y. (2016). Development and implementation of a micro-electric discharge machine: Real-time monitoring system of fabrication of nanosilver colloid. *Journal of Cluster Science, 27*, 763–773.

Unune, D. R., Singh, V. P., & Mali, H. S. (2016). Experimental investigations of abrasive mixed electro discharge diamond grinding of nimonic 80A. *Materials and Manufacturing Processes, 31*, 1718–1723.

Wong, Y. S., Rahman, M., Lim, H. S., Han, H., & Ravi, N. (2003). Investigation of micro-EDM material removal characteristics using single RC-pulse discharges. *Journal of Materials Processing Technology, 140*, 303–307.

Yadav, R. N., Yadava, V., & Singh, G. K. (2014). Application of non-dominated sorting genetic algorithm for multi-objective optimization of electrical discharge diamond face grinding process. *Journal of Mechanical Science and Technology, 28*, 2299–2306.